Comparison of Structure Parameter Scaling Expressions with Turbulence Closure Model Predictions

STEPHEN D. BURK

Naval Environmental Prediction Research Facility, Monterey, CA 93940

(Manuscript received 26 June 1980, in final form 18 December 1980)

ABSTRACT

The convective boundary-layer scaling expressions presented by Wyngaard and LeMone (1980) are compared with predictions from a turbulence closure model. We first examine a model experiment involving a clear-air, convectively driven boundary layer overland. The model results agree well with scaling expressions and observations in the lower boundary layer and near the inversion. In the mid-boundary layer region, however, the closure model underestimates the temperature structure parameter C_T^2 and overestimates the humidity structure parameter C_q^2.

A cloud-topped marine boundary layer is examined in a second experiment which uses AMTEX data. Order-of-magnitude differences are found here between interfacial-layer scaling expressions and closure model predictions. Potential sources of this disagreement are discussed.

1. Introduction

In a recent paper, Wyngaard and LeMone (1980, hereafter referred to as WL) examine existing scaling expressions for the refractive index structure parameter in the surface and mixed layers, and they develop new scaling expressions for the entraining region of the convective boundary layer. Burk (1980) discusses the computation of structure parameter profiles in the boundary layer using a second-moment closure model. Here we compare the scaling law expressions with results from the turbulence closure model, and focus particular attention on results in the interfacial region of the convective boundary layer where the new WL formulations are applicable.

Details concerning the general nature of the refractive index structure parameter are presented in WL and Burk (1980), and in references contained therein. For our purposes here we note only that the refractive index structure parameter may be expressed in a general way as

$$C_n^2 = B_1 C_T^2 + B_2 C_{Tq} + B_3 C_q^2. \qquad (1)$$

Here C_T^2 and C_q^2 are the structure parameters for temperature and specific humidity, and C_{Tq} is the structure parameter describing the temperature-humidity cospectrum. The weighting coefficients B_1, B_2 and B_3 involve temperature, pressure and well-known constants. These weighting coefficients differ for acoustic, optical and microwave propagation. Thus, when computing the refractive index structure parameter, either from scaling laws or a closure model, one generally first computes the individual temperature and humidity structure parameters.

Section 2 contains a brief model description and discussion of the numerical experiments conducted. Results from these experiments are presented in Section 3 and compared with the WL findings. Concluding remarks are presented in Section 4.

2. Description of the model and the experiments

As discussed in Burk (1980), this model is one-dimensional and uses the Mellor and Yamada (1974) level-3 formulation.[1] The triple-correlation terms are written in a downgradient diffusion fashion, e.g.,

$$-\overline{w'(f')^2} = K \frac{\overline{\partial f'^2}}{\partial z}, \qquad (2)$$

where w' is the fluctuating vertical velocity and f any one of the model variables of interest. The overbar represents an ensemble average. Here K acts as an eddy coefficient, being composed of the product of a length scale and a velocity scale. As noted by Wyngaard (1973) and Lumley *et al.* (1978), such downgradient modeling of the triple-moment terms is inadequate for buoyancy driven flow. Modeling these terms along the lines of Lumley and Khajeh-

[1] This level-3 model has prognostic equations for the wind components, liquid-water potential temperature, total moisture specific humidity, turbulent kinetic energy, the variances of temperature and humidity, and the temperature-humidity covariance. The remaining second-moment equations are solved diagnostically.

Nouri (1974), albeit more complex, would be more appropriate for the convective boundary layer. Our intention here, however, is to compare model predictions with the WL scaling formulation which finds the triple-moment transport terms to be of negligible importance. Thus, the shortcomings of the downgradient diffusion closures may not be of major importance.

Considerable effort has been expended on improving closure assumptions used in second-order turbulence models and, in the process, several groups have developed third-order closure schemes (André *et al.*, 1976; Zeman and Lumley, 1976). Although one must acknowledge that improvements are warranted for assumptions used in current level-3 turbulence models such as used here, nevertheless, it seems logical to check the results of an available, working model with observational data and with other proposed formulations before engaging in another cycle of model refinement. Here our primary intent is to compare with the WL scaling expressions, which themselves contain simplifying assumptions that warrant independent scrutiny. For example, WL assume quasi-steady conditions, introduce approximations to the turbulence budget equations, and use a mean-field closure which involves specifying the shape of the mean temperature and humidity profiles throughout the interfacial layer.

Comparison of the turbulence model results with other formulations should not be misconstrued as implying that we consider the closure model to be the benchmark by which other schemes are to be measured. Rather, we wish to establish the extent of agreement (or lack thereof) between the numerical model, the various scaling laws, and observational data. This approach can provide a rational basis for evaluating what further model refinements may be necessary.

The temperature and moisture structure parameters in Eq. (1) are computed with the closure model by recasting relations such as that developed by Corrsin (1951),

$$C_T^2 = \beta \chi_T \epsilon^{-1/3}, \tag{3}$$

into forms which directly involve variables of the level-3 model. Here χ_T is the molecular destruction rate of temperature variance, ϵ is the dissipation rate of turbulent kinetic energy, and β is an empirical constant having a value of about 1.6. In developing the closure model (Mellor, 1973), closure assumptions on χ_T and ϵ were made. For consistency, we use the same closure assumptions in Eq. (3) and find (Burk, 1980), i.e.,

$$C_T^2 = \gamma \overline{T'^2} \lambda^{-2/3}, \tag{4}$$

where γ is a constant, T' fluctuating temperature, and λ a macroscale characteristic of the energy carrying eddies. Expressions similar to Eq. (4) involving moisture variance and the temperature-moisture covariance are developed for C_q^2 and C_{Tq}. Thus, we are in a position to evaluate Eq. (1) with the closure model for a variety of boundary-layer simulations. Since our interest here is to compare with the convective scaling expressions discussed in WL, we restrict our attention to two numerical experiments, each involving a convective boundary layer. If the results here are encouraging, then we anticipate use of such a closure model in aiding the development of scaling laws for more complex boundary-layer situations (e.g., where baroclinity and wind shear are important).

The length scale used in Eq. (4) is taken to be similar to that suggested by Mellor and Yamada (1974), *viz.*,

$$\lambda = \frac{kz}{1 + kz/\lambda_0},$$

where

$$\lambda_0 = 0.1 \frac{\int_0^\infty zedz}{\int_0^\infty edz}.$$

Here k is von Kármán's constant, z height, and e the square root of twice the turbulent kinetic energy. We add to this prescription of λ a modification to account for the influence of stable stratification on the length scale as discussed by André *et al.* (1978). In stable regions (where $\partial\Theta_v/\partial z$ is positive), we compute the length scale λ_s by

$$\lambda_s = 0.53e\left(\frac{g}{T_0}\frac{\partial\Theta_v}{\partial z}\right)^{-1/2}.$$

The actual length scale used in stable regions is the smaller of λ and λ_s. Here g is gravitational acceleration, T_0 a reference temperature, and Θ_v the virtual potential temperature.

Eq. (4) indicates that the length scale is a very important parameter in the determination of structure parameters. The exact functional dependence of C_T^2, for example, on λ, however, is difficult to establish because the temperature variance is related to λ in a complex manner through budget expressions. Turbulence models which carry their own budget equations for λ or for the dissipation rate ϵ would appear to have a significant advantage over the method of prescribing λ described here. This advantage, however, is difficult to realize because every term in the dynamic equation for λ or ϵ must be modeled. Thus, compared to the other second-moment budget equations which have major terms

that require no modeling, a modeled dynamic length-scale equation contains a considerable degree of arbitrariness. Lewellen (1977) discusses this point further in a review of invariant modeling. In any case, we must ultimately judge any scheme, no matter how sophisticated its appearance and appealing its parameterizations, by comparison with observational data.

The first numerical experiment to be discussed concerns a cloud-free overland convective boundary layer. The model is initialized at 2000 LT and integrated through the afternoon of the following day, with the surface temperature specified to undergo a diurnal oscillation. We examine the model output in midafternoon when the boundary layer is very unstable and compare model-computed structure parameter profiles with the scaling law expressions and observations. The initial and boundary conditions are identical with those discussed in Burk (1977) except that a smaller geostrophic wind speed (5 m s^{-1}) is used so as to assure development of a strongly convective boundary layer.

The second numerical experiment simulates a convective marine planetary boundary layer (PBL) using data from the Air Mass Transformation Experiment (AMTEX) to initialize the model. Initial potential temperature and specific humidity profiles are taken from Fig. 1 of Wyngaard *et al.* (1978). Simultaneous wind profiles for the 15 February 1975 AMTEX flights are unreported, so the model's value of geostrophic wind was adjusted to yield the observed surface stress value (Wyngaard *et al.*, 1978, Table 1). Similarly, the model's sea surface temperature was adjusted so as to yield the observed surface temperature flux. Without further constraint, the model computes a surface moisture flux having a value very close to the observed.[2] Thus, these initial and boundary conditions should assure a faithful simulation of boundary-layer characteristics in the AMTEX region.

This marine PBL experiment develops considerable cloudiness. The associated boundary layer turbulence properties and structure parameter characteristics differ significantly from the dry, overland experiment.

3. Model results and comparisons with WL

a. Overland experiment

Midafternoon turbulent structure of the convectively driven boundary layer (Monin-Obukhov length

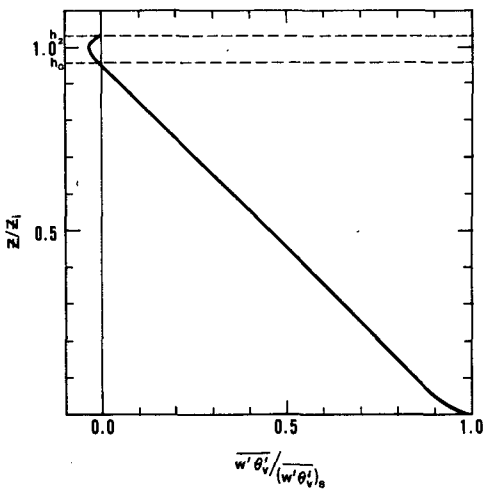

FIG. 1. Midafternoon profile of mean virtual potential temperature flux from the overland simulation. The zero crossing points of $\overline{w'\theta_v'}$ define the base (h_0) and top (h_2) of the interfacial layer.

= −7.2 m) is examined in this case. The inversion is located at 1740 m and the virtual temperature flux is linear throughout the well-mixed boundary layer (Fig. 1). As in WL, we use the zero crossing points of the virtual temperature flux (taken from closure model results) to delineate the interfacial layer wherein the new WL scaling formulation is applicable. Here h_0 = 1675 m and h_2 = 1795 m, where these h values refer to the heights of the base and top of the interfacial layer. The specific humidity distribution has a sharp decrease within the interfacial layer, with this case satisfying the large $|\Delta q|$ assumption used by WL in developing their scaling expressions; *viz.*, $|\Delta q| \gg |(q, 3)_2|\Delta h$ [here $(q, 3)_2$ is the vertical derivative of specific humidity evaluated at h_2, $\Delta h = h_2 - h_0$ and $\Delta q = q_2 - q_0$].

The moisture flux $\overline{w'q'}$ has a uniform increase with height in the mixed layer which is indicative of the boundary layer drying (Fig. 2). This drying is caused by entrainment of dry air from aloft into the growing boundary layer. The curvature in the moisture flux profile near the surface results from the surface specific humidity being sent, in this case, through a diurnal wave which is in phase with the surface temperature wave (Burk, 1977). The surface specific humidity is near a maximum and the surface layer is moistening. Within the interfacial layer near the inversion, the moisture flux shows a monotonic decrease.

As noted by WL, within the lower portion of a convectively driven boundary layer, the structure parameters follow mixed-layer scaling,

$$\frac{C_T^2 Z_i^{2/3}}{\theta_*^2} = A(Z/Z_i)^{-4/3}, \qquad (5)$$

[2] W. S. Lewellen performed a similar numerical experiment with this AMTEX data in his investigation of the transport characteristics of water vapor. *Proc. Workshop on Atmospheric Water Vapor*, A. Deepak, Ed., Vail, CO, 11–13 September 1979, Inst. for Atmos. and Remote Sensing.

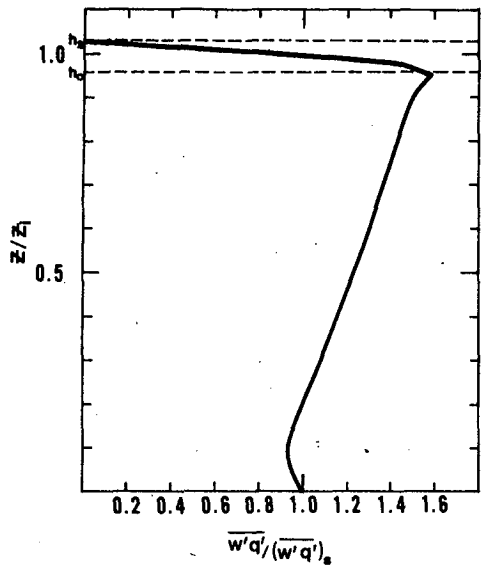

FIG. 2. As in Fig. 1 except for specific humidity flux.

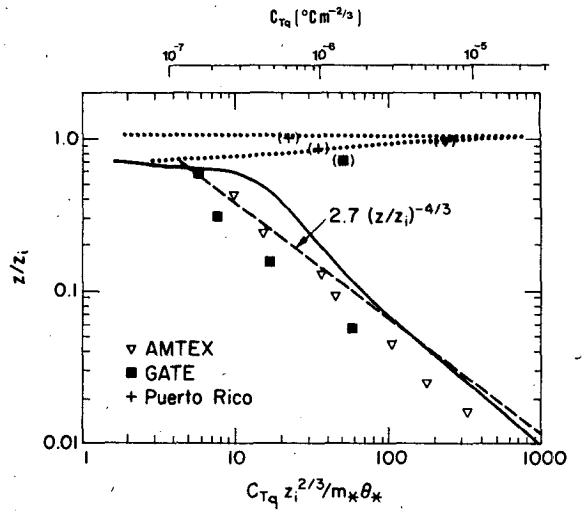

FIG. 4. As in Fig. 3 except for temperature-humidity structure parameter. The dotted line is for negative values of model-predicted C_{Tq}. Data values in parentheses are negative.

$$\frac{C_{Tq}Z_i^{2/3}}{\theta_* m_*} = B(Z/Z_i)^{-4/3}, \tag{6}$$

$$\frac{C_q^2 Z_i^{2/3}}{m_*^2} = C(Z/Z_i)^{-4/3}, \tag{7}$$

where A, B and C are empirical constants.[3] Due to entrainment effects, however, large departures from these scaling expressions occur as the inversion is approached. The closure model predictions for C_T^2 in this experiment follow the $Z^{-4/3}$ scaling to a height of $\sim 0.3Z_i$; decrease somewhat more rapidly with height in the region $0.3Z_i < Z < 0.7Z_i$; and then exhibit a peak at Z_i (Fig. 3). Also shown in Fig. 3 is the collection of data points used by WL. While it is gratifying that the closure model yields results in good agreement with the data in the lower portion of the boundary layer and near the inversion, the apparent underestimation of C_T^2 in the mid-boundary-layer region is disturbing. This underestimation may be associated with the inadequacy of the triple-moment closure assumptions, but this point needs further investigation. The situation is further complicated by the fact that the scaled observational data show considerable scatter in the mid and upper region of the boundary layer, indicating that mixed layer $Z^{-4/3}$ scaling isn't working. Thus, comparison of model results and scaled data in this region can be difficult. As we will see, the WL scaling provides a very useful method of unifying and interpreting the observations and model results within the interfacial layer. No such unity appears between model results and observations when interfacial layer results are plotted in mixed layer scales.

Observed values of C_{Tq} follow $Z^{-4/3}$ scaling throughout the lower half of the boundary layer. However, due to the entrainment of warm, dry air, the sign of C_{Tq} changes as the inversion is approached and C_{Tq} shows a peak near Z_i. Closure model results here are in good agreement with the observations (Fig. 4). As noted by WL, however, observations indicate that B in Eq. (6) is closer to 2.0 than to 2.7, which is the value of A in Eq. (5). That this difference in the magnitude of the coefficient does not appear in the closure model results is likely due

[3] See the Appendix for list of symbols.

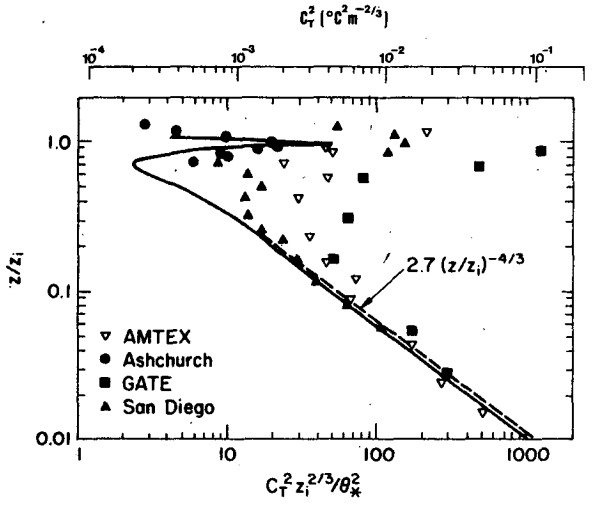

FIG. 3. Model-computed midafternoon temperature structure parameter distribution normalized by mixed-layer scales (solid line). Dashed line is the mixed-layer scaling prediction [Eq. (5)]. Collection of individual data points is taken from Wyngaard and LeMone (1980). Upper scale applies only to solid line.

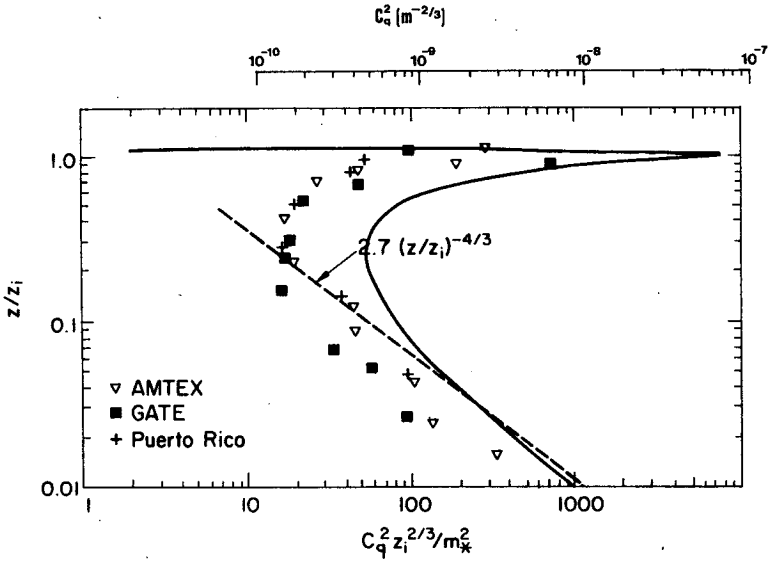

FIG. 5. As in Fig. 3 except for humidity structure parameter.

to the assumption inherent in the level-3 model that water vapor and heat are transported identically.

Observed C_q^2 values appear to follow mixed-layer scaling through only a shallow depth, perhaps 0.1–0.2Z_i. Entrainment affects the C_q^2 distribution throughout the remainder of the boundary layer, with a substantial peak occurring at Z_i. The closure model captures these general features of the observed C_q^2 distribution (Fig. 5), but shows overestimation of C_q^2 in the mid-boundary-layer region. Also, it is not clear to what extent this overestimate is real and to what extent it is a result of the breakdown of mixed-layer scaling. Data also indicate that the coefficient C in Eq. (7) is probably smaller than A (=2.7).

We turn now to comparison of closure model results with the WL formulations for the interfacial layer. The WL scaling takes the form of layer-averaged values (indicated by angular braces) within the interfacial layer:

$$\langle C_T^2 \rangle = \frac{T_i \theta_{v*}}{Z_i^{2/3}}, \tag{8}$$

$$\langle C_{Tq} \rangle = \frac{Q_i \theta_{v*}}{Z_i^{2/3}}, \tag{9}$$

$$\langle C_q^2 \rangle = \frac{3.9(\rho \Delta q)^2 \theta_{v*}}{Z_i^{2/3} \Delta \Theta_v}, \tag{10}$$

where

$$Q_i = \rho \Delta q \left[2.2 - \frac{2.4T}{\Delta \Theta_v} \Delta q \right],$$

$$T_i = \Delta \Theta_v \left[0.5 - \frac{2.6T}{\Delta \Theta_v} \Delta q + 1.4 \left(\frac{T}{\Delta \Theta_v} \Delta q \right)^2 \right].$$

Note that we rewrite the WL expressions in terms of specific humidity q throughout rather than using absolute humidity as in WL.

From the closure model results we can compute these WL layer-averaged values and compare with the computed closure model structure parameters in the interfacial layer. Table 1 presents the model values necessary to evaluate Eqs. (8)–(10), along with the resultant layer-averaged values. Profiles of model computed structure parameters within the interfacial layer are shown in Fig. 6. If the closure model results and the WL scaling were in full agreement, then the average value of each structure parameter profile within the interfacial layer in Fig. 6 would equal 1.0. This is close to true for the scaled C_T^2 values; the interfacial average of the model prediction is seen to be about 0.9. For C_q^2 the average scaled value in Fig. 6c is near 0.6, and that for C_{Tq} is intermediate between the C_T^2 and C_q^2 averages. This factor of 2 or better agreement, while perhaps unimpressive, should properly be viewed in terms of

TABLE 1. Model output values used to evaluate Eqs. (8)–(10) and Eqs. (12)–(13) in overland case along with resultant average values.

θ_{v*}	0.119°C
Z_i	1740 m
Δq	-2.84×10^{-3}
$\Delta \Theta_v$	0.5°C
$T(h_0)$	11.0°C
$(\overline{w'\theta_v'})_s$	0.307 m °C s^{-1}
h_0	1675 m
$\langle C_T^2 \rangle$	3.43×10^{-3} °C^2 m$^{-2/3}$
$\langle C_{Tq} \rangle$	-1.6×10^{-5} °C m$^{-2/3}$
$\langle C_q^2 \rangle$	6.6×10^{-8} m$^{-2/3}$

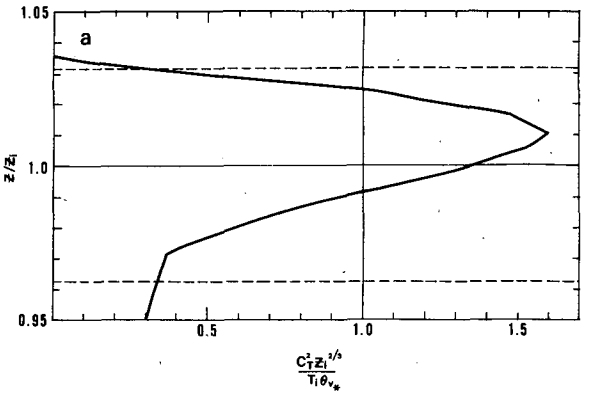

FIG. 6a. Model predicted C_T^2 values in the overland case normalized with the interfacial-layer scales of Wyngaard and LeMone (1980). Dashed lines delineate interfacial layer.

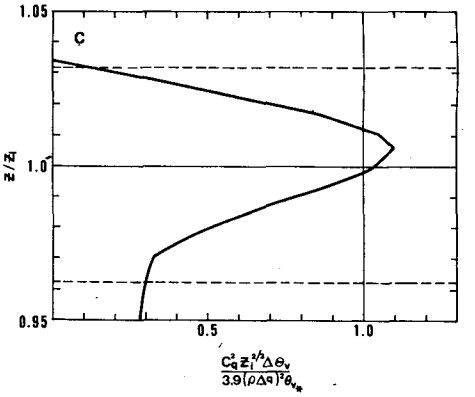

FIG. 6c. As in Fig. 6a except for scaled C_q^2.

the several orders of magnitude variations in C_T^2, C_{Tq} and C_q^2 across the boundary layer. Further, due to the intermittent nature of turbulence near the inversion, properly averaged structure parameter measurements are very difficult to make. A factor of 2 agreement with several different measurement systems would probably be quite acceptable. Thus, the degree of agreement here is very encouraging, particularly because the WL scaling expressions [Eqs. (8)–(10)] offer an attractive method of estimating layer-averaged structure parameter values using quantities either routinely available or easily computed from bulk measurements. For example, in the marine environment, a ship sounding yields an estimate of Z_i, $\Delta\Theta_v$ and Δq, while measured wind, humidity and air-sea temperature differences, when combined with bulk turbulence formulas, permit estimates of θ_{v*}. Furthermore, and somewhat surprisingly, the turbulence model results here compare more favorably with the WL interfacial layer scaling than they do with $Z^{-4/3}$ mixed-layer scaling in the mid to upper regions of the boundary layer. We say this is somewhat surprising because it is in the interfacial layer where we would have anticipated the most difficulties arising from closure assumptions—both second-order and mean-field closures.

It is also worthwhile to compare turbulence model interfacial averages of the individual dissipation rates with the WL expressions. As an example, consider the WL equation

$$\langle C_q^2 \rangle \approx 1.6\langle \epsilon \rangle^{-1/3} \langle \chi_q \rangle, \tag{11}$$

where χ_q is the molecular destruction rate of humidity fluctuations. Approximations for the terms in Eq. (11) are derived by WL to be

$$\langle \chi_q \rangle_{\mathrm{WL}} \approx \frac{17(\rho\Delta q)^2(\overline{w'\theta_v'})_s}{15 h_0 \Delta\Theta_v}, \tag{12}$$

$$\langle \epsilon \rangle_{\mathrm{WL}} \approx 0.2 \frac{g}{T}(\overline{w'\theta_v'})_s. \tag{13}$$

Substitution of values from Table 1 into Eqs. (12)–(13) gives $\langle \chi_q \rangle_{\mathrm{WL}} = 4.3 \times 10^{-9}$ s^{-1} and $\langle \epsilon \rangle_{\mathrm{WL}} = 2.1 \times 10^{-3}$ m^2 s^{-3}.

Table 2 contains the closure model computed values of ϵ and χ_q at the grid points lying within the interfacial layer and their average values within the layer as computed by trapezoidal integration. [As a

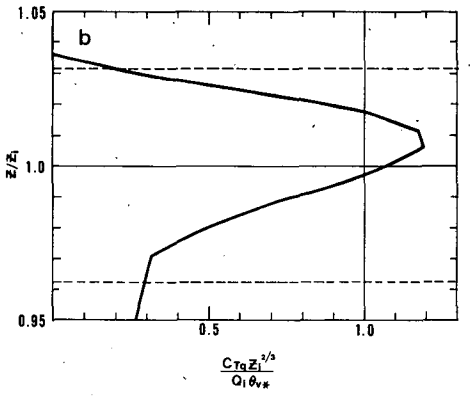

FIG. 6b. As in Fig. 6a except for scaled C_{Tq}.

TABLE 2. Model output values of ϵ and χ_q within interfacial layer in overland case and computed layer averages.

Z (m)	ϵ (m^2 s^{-3})	χ_q (s^{-1})	$\langle\epsilon\rangle$	$\langle\chi_q\rangle$
1680	7.14×10^{-4}	9.14×10^{-10}	1.1×10^{-3}	2.5×10^{-9}
1690	6.75×10^{-4}	9.38×10^{-10}		
1700	9.05×10^{-4}	1.38×10^{-9}		
1710	1.18×10^{-3}	2.02×10^{-9}		
1720	1.40×10^{-3}	2.73×10^{-9}		
1730	1.55×10^{-3}	3.43×10^{-9}		
1740	1.58×10^{-3}	3.97×10^{-9}		
1750	1.50×10^{-3}	4.13×10^{-9}		
1760	1.28×10^{-3}	3.75×10^{-9}		
1770	9.45×10^{-4}	2.79×10^{-9}		
1780	5.37×10^{-4}	1.50×10^{-9}		
1790	1.77×10^{-4}	4.53×10^{-10}		

consistency check, substitution of $\langle \epsilon \rangle$ and $\langle \chi_q \rangle$ from Table 2 into Eq. (11) gives 3.9×10^{-8} m$^{-2/3}$, which is in good agreement with a direct layer average of model C_q^2 values (Fig. 6c).]

Thus, taking the ratio of the values computed from Eqs. (12)–(13) and the direct model averaged values from Table 2 gives

$$\left.\begin{aligned} \frac{\langle \chi_q \rangle_{WL}}{\langle \chi_q \rangle} &= 1.7 \\ \frac{\langle \epsilon \rangle_{WL}}{\langle \epsilon \rangle} &= 1.9 \\ \frac{\langle C_q^2 \rangle_{WL}}{\langle C_q^2 \rangle} &= \frac{\langle \chi_q \rangle_{WL}}{\langle \chi_q \rangle} \frac{\langle \epsilon \rangle^{1/3}}{\langle \epsilon \rangle_{WL}^{1/3}} = 1.4 \end{aligned}\right\}$$

Interestingly, because of the functional form of $\langle C_q^2 \rangle$, the final ratio above is the one most nearly unity. A goal of future work in this area certainly must be to attain ratios of the interfacially averaged dissipation terms (scaling formulation to turbulence model results) more nearly unity.

Finally, we note that $\langle C_q^2 \rangle_{WL}$ computed from Eqs. (11)–(13) is 5.4×10^{-8} which is 18% smaller than the value (Table 1) computed from Eq. (10). This discrepancy occurs because (10) contains the WL assumption that $h_0 = 0.8Z_i$, while (11)–(13) do not.

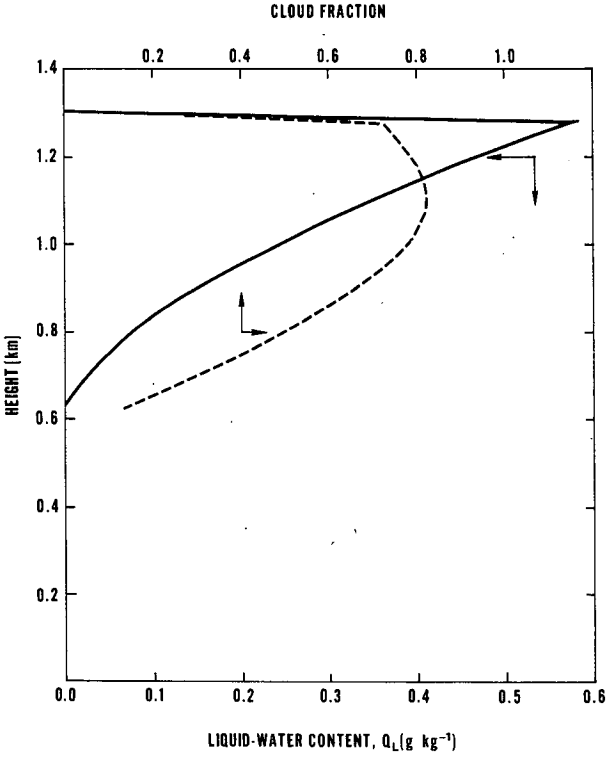

FIG. 7. Distribution of liquid water (lower scale, solid line) and cloud fraction (upper scale, dashed line) from AMTEX simulation.

TABLE 3. Model output values used to evaluate Eqs. (8)–(10) in AMTEX simulation along with resultant average values.

θ_{v*}	0.085°C
Z_i	1313 m
Δq	-3.47×10^{-3}
$\Delta\Theta_v$	2.5°C
$T(h_0)$	−0.5°C
$\langle C_T^2 \rangle$	3.0×10^{-3} °C^2 m$^{-2/3}$
$\langle C_{Tq} \rangle$	-7.7×10^{-6} °C m$^{-2/3}$
$\langle C_q^2 \rangle$	1.3×10^{-8} m$^{-2/3}$

At the time at which we are examining model output in this numerical experiment, $h_0 \approx 0.96Z_i$.

b. AMTEX simulation

As discussed in Section 2, in this case the initial conditions come from data gathered on 15 February 1975 during the AMTEX experiment and reported by Wyngaard *et al.* (1978). The model predicts cloudiness throughout most of the upper half (~700–1300 m) of the boundary layer. The model contains the Gaussian cloud model relations developed by Sommeria and Deardorff (1977) and Mellor (1977); hence, the cloud fraction is also predicted. Fig. 7 shows that the model-computed maximum in-cloud liquid water content is 0.58 g kg^{-1} and the cloud fraction maximum is 0.82. These results apparently are in general agreement with the Wyngaard *et al.* (1978) statement that clouds typically were present in the upper few hundred meters of the boundary layer over as much as 80% of the AMTEX area. Further, the fact that the model cloud fraction is substantially less than 1 throughout the cloudy region is indicative of convective rather than stratus-type clouds.

When model-predicted C_T^2 values are scaled by mixed-layer parameters, the same general features occur in this experiment as in the previous case (Table 3 contains model output parameters used for scaling). The lower portion of the boundary layer shows a $Z^{-4/3}$ dependence, C_T^2 values are underestimated at midboundary layer, and a peak occurs in C_T^2 near the inversion (Fig. 8). Here the peak is an order of magnitude stronger than previously, being associated with the strong turbulent activity near cloud top. Such in-cloud enhancement of the structure parameters has significant implications for the radar reflectivities of clouds (Gossard, 1979).

The scaled profile of C_{Tq} has a more complex structure here than in the previous experiment. The $Z^{-4/3}$ distribution in the lower boundary layer gives way to a small region of negative C_{Tq} near cloud base. In the bulk of the cloud layer, C_{Tq} is again positive. Then, a negative peak occurs at cloud top (Fig. 9).

The distribution in Fig. 9 can be understood qualitatively in terms of mixing in the presence of mean gradients of potential temperature and specific

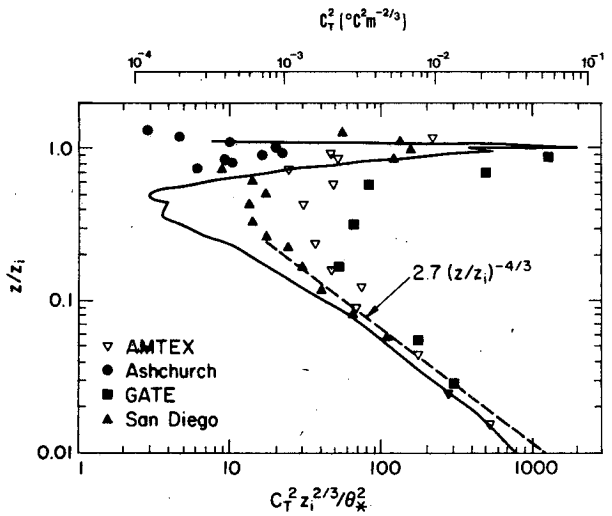

FIG. 8. Model-computed temperature structure parameter distribution in AMTEX simulation normalized by mixed-layer scales (solid line). Dashed line is the mixed-layer scaling prediction. Collection of individual data points is taken from Wyngaard and LeMone (1980). Upper scale applies only to solid line.

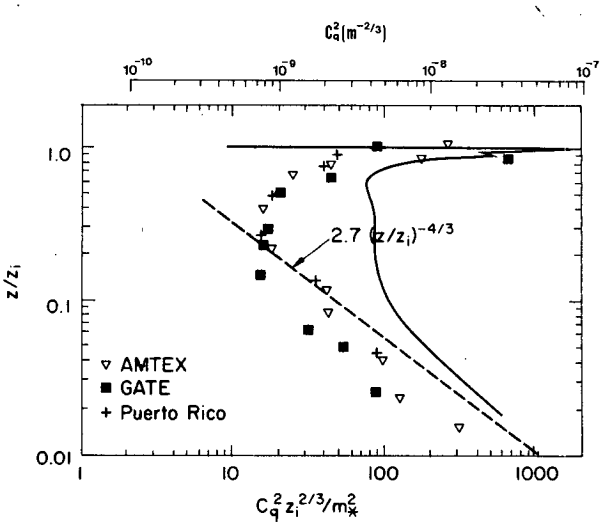

FIG. 10. As in Fig. 8 except for humidity structure parameter.

humidity. In the lower boundary layer there is a slight decrease in potential temperature and specific humidity with height. Parcels originating a small distance l above or below some reference level Z_r arrive at Z_r either cooler and drier, or warmer and more moist, respectively, than the environment at Z_r. Thus, the temperature-moisture correlation associated with turbulent fluctuations in this region is positive, which means that C_{Tq} will be positive. Slightly beneath cloud base, potential temperature shows an increase with height, while specific humidity continues to decrease with height. In this thin region, parcels coming down a distance l from above have a negative correlation (warmer and drier than their surroundings), and those traveling upward a distance l and then mixing at the level of interest will also have a slightly negative (cooler and more moist) correlation. A net negative correlation in this region, such as shown in Fig. 9, therefore, seems reasonable.

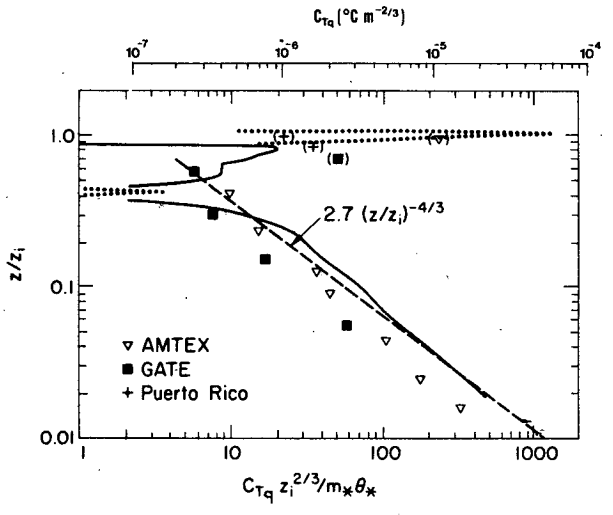

FIG. 9. As in Fig. 8, except for temperature-humidity structure parameter. The dotted line is negative values of model-predicted C_{Tq}. Data values in parentheses are negative.

Within the cloud layer the lapse rate is between the moist adiabatic and dry adiabatic value. Specific humidity decreases with height. Consideration of cloud parcels which are rising and falling while following moist adiabats results in the conclusion that the in-cloud temperature-moisture correlation should be positive.

Finally, entrainment of warm, dry air from above the inversion accounts for the strong, negative C_{Tq} peak at cloud top (Fig. 9).

The distribution of C_q^2 in this AMTEX simulation is similar to that discussed in the overland case. However, here we see an even stronger apparent overestimation of C_q^2 in the midboundary layer region (Fig. 10) as compared to the scaled observational data. The $Z^{-4/3}$ mixed-layer scaling, however, clearly is not working in midboundary layer, which makes comparison of scaled data with model results hazardous.

If we now look in detail at the structure parameters within the interfacial layer, we find considerable differences here as compared to the overland experiment. In the previous case, interfacial layer averages of the model predictions were within a factor of 2 of those predicted by the WL approximations. Here the model's layer average values are considerably larger than that predicted by the WL formulation (Fig. 11). This disagreement is particularly large for scaled values of C_T^2.

Much of the disagreement here between closure model and WL scaling values may arise from the presence of clouds. The WL interfacial formulations are derived assuming a clear, convective boundary layer and neglecting radiation. Assumptions such as a monotonic, linear decrease in virtual potential temperature flux with height between the surface and h_0, used in deriving the WL interfacial-layer expressions, are inapplicable to a cloud-topped boundary layer. Nevertheless, WL compare their scaling expressions against the AMTEX data set among others, and further show their scaling to be in good agreement with the AMTEX data.

Perhaps the agreement of the clear-air WL expressions and the AMTEX data is due to preferential sampling by the aircraft. Apparently, due to instrumentation difficulties caused by cloud water, an effort was made to avoid flying through clouds. In their earlier article, Wyngaard *et al.* (1978) specifically excluded consideration of AMTEX data in the interfacial layer because of these aircraft sampling difficulties. The closure model results represent ensemble averages and contain no bias as to whether a region is cloudy or not. Direct comparisons with the AMTEX aircraft data in the upper boundary layer therefore may not be possible. Lewellen[2] also makes this point in his discussion of an AMTEX modeling experiment.

4. Discussion

WL do not expect their expressions for interfacial layer-average structure parameter values to contain uncertainties exceeding a factor of 2. Their approximations to the variance budgets and their mean-field closure represent the most likely error sources. Indeed, in our overland, clear-air experiment, the layer-average values predicted by the closure model are within a factor of 2 of what the WL expressions would predict. A significant portion of the remaining discrepancy may be due to the closure assumptions, such as the model's use of downgradient diffusion for the triple-moment transport terms. Thus, when we restrict our attention to clear, buoyancy driven boundary layers, the agreement between observational data, interfacial scaling laws, and closure model predictions is encouraging. Tests of closure model results in a wider variety of boundary layer situations appears warranted.

There is a significant portion of the convective boundary layer, lying between the surface and the interfacial layer, for which $Z^{-4/3}$ mixed-layer scaling does not work. This is evidenced by the wide scatter of the data away from the $Z^{-4/3}$ line in Figs. 3–5. Thus, in this region, some of the disagreement between closure model results and the data points may be attributable to the inadequacy of mixed-layer scaling. For example, the closure model's peak

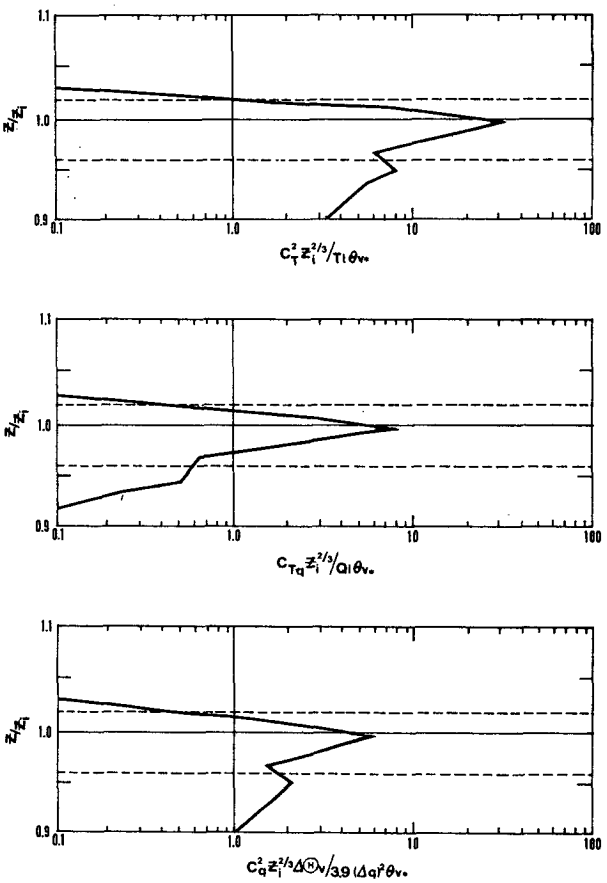

FIG. 11. Model-predicted structure function values in the AMTEX simulation normalized with the interfacial-layer scales of Wyngaard and LeMone (1980). Dashed lines delineate interfacial layer.

value of C_q^2 near the inversion when plotted in mixed-layer scales is much larger than any of the data points plotted (Fig. 5). However, as we have seen, when the data and closure model results in the interfacial layer are instead scaled in the manner proposed by WL, then the agreement is good. The fact, however, that the model C_T^2 profile decreases more rapidly than $Z^{-4/3}$ in the region $0.3Z_i \leq Z \leq 0.7Z_i$ while the observed data falls on the other side of the $Z^{-4/3}$ line appears to be more than just a scaling difficulty and requires further attention.

For examination of cloud-topped boundary layers more general scaling expressions must be developed. The WL interfacial-layer expressions are derived assuming a nonradiating, cloud-free boundary layer. It is not surprising, therefore, that we find as much as an order-of-magnitude disagreement between closure model predictions and WL scaling expressions in our cloudy AMTEX simulation. Despite their stated restriction to clear-air boundary layers, WL compare their scaling expressions with data from the cloudy AMTEX boundary layer and,

furthermore, they show good agreement with the AMTEX data. This good agreement may be a result of preferential sampling by the aircraft of the clear air, which is the region of validity of WL scaling.

Although complex and computationally expensive, closure modeling offers a general approach to computing structure parameter profiles for a variety of atmospheric stabilities, both in cloudy and cloud-free boundary layers (Burk, 1980). Working in close conjunction with observational data, the closure model may aid in development of simpler scaling expressions, valid for a wide range of atmospheric conditions. Further, the mixed-layer model developed by Lilly (1968) in his study of stratus-capped boundary layers might provide useful insight into methods of generalizing the WL approach. Thus, we appear to be in a fortunate position in which a wide range of boundary layer techniques, experimental and theoretical, can be brought to bear on the problem of understanding and predicting refractive index structure parameter behavior.

Acknowledgments. The author thanks Dr. Paul Tag for helpful comments on the manuscript. Thanks also are extended to Mr. Steve Bishop for editorial assistance, to Ms. Winona Carlisle for typing the manuscript, and to DM1 Frank Hermoso for drafting the figures.

APPENDIX

List of Symbols

Roman symbols

A, B, C	coefficients in mixed-layer scaling [Eqs. (5)–(7)]
B_1, B_2, B_3	weighting coefficients in refractive index structure parameter expression [Eq. (1)]
C_n^2, C_q^2, C_T^2	structure parameters for refractive index, specific humidity and temperature, respectively
C_{Tq}	joint temperature-humidity structure parameter
e	square root of twice the turbulent kinetic energy
f	any model variable for which downgradient diffusion assumption is made, Eq. (2)
g	acceleration of gravity
h_0, h_2	base and top of interfacial layer ($h_0 < h_2$)
k	von Kármán's constant
K	eddy coefficient in downgradient diffusion expression [Eq. (2)]
m_*	mixed layer humidity scaling factor $[=(\overline{w'q'})_s/w_*]$
n	refractive index
q	specific humidity
Q_i	interfacial layer humidity scale [Eq. (9)]
T	absolute temperature
T_i	interfacial layer temperature scale [Eq. (8)]
w'	fluctuating vertical velocity
w_*	mixed-layer scaling velocity
Z	height
Z_i	inversion height.

Greek symbols

β	constant in Corrsin expression for C_T^2 [Eq. (3)], taken as 1.6
γ	Constant in closure model C_T^2 expression [Eq. (4)], [see Burk, 1980, Eq. (22)]
ϵ	molecular dissipation rate of turbulent kinetic energy
λ	a macroscale characteristic of the energy carrying eddies [Eq. (4)]
θ'	fluctuating potential temperature
Θ_v	mean virtual potential temperature
θ_*	mixed layer temperature scale $[=(\overline{w'\theta'})_s/w_*]$
χ_q, χ_T	molecular destruction rate of humidity and temperature fluctuations, respectively.

Other symbols

$(\ )_0$	at height h_0
$(\ )_2$	at height h_2
$(\ )_s$	surface
$(\ )_v$	virtual
$\langle\ \rangle$	interfacial-layer average
$\Delta(\ )$	$(\ )_2 - (\ )_0$
$(\ , 3)$	vertical derivative
$\overline{(\ )}$	ensemble average
$(\ )'$	fluctuation from the mean.

REFERENCES

André, J. C., G. De Moor, P. Lacarrére and R. Du Vachat, 1976: Turbulence approximation for inhomogeneous flows: Part I. The clipping approximation. *J. Atmos. Sci.*, **33**, 476–481.

——, ——, ——, G. Therry and R. Du Vachat, 1978: Modeling the 24-hour evolution of the mean and turbulent structures of the planetary boundary layer. *J. Atmos. Sci.*, **35**, 1861–1883.

Burk, S. D., 1977: The moist boundary layer with a higher order turbulence closure model. *J. Atmos. Sci.*, **34**, 629–638.

——, 1980: Refractive index structure parameters: Time-dependent calculations using a numerical boundary layer model. *J. Appl. Meteor.*, **19**, 562–576.

Corrsin, S., 1951: On the spectrum of isotropic temperature fluctuations in an isotropic turbulence. *J. Appl. Phys.*, **22**, 469–473.

Gossard, E. E., 1979: A fresh look at the radar reflectivity of clouds. *Radio Sci.*, **14**, 1089–1097.

Lewellen, W. S., 1977: Use of invariant modeling. *Handbook of Turbulence*, W. Frost and T. H. Moulden, Eds., Plenum Press, 237–280.

Lilly, D. K., 1968: Models of cloud-topped mixed layers under a strong inversion. *Quart. J. Roy. Meteor. Soc.*, **94,** 292–309.

Lumley, J. L., and B. Khajeh-Nouri, 1974: Computational modeling of turbulent transport. *Advances in Geophysics*, Vol. 18A, Academic Press, 169–192.

——, O. Zeman and J. Siess, 1978: The influence of buoyancy on turbulent transport. *J. Fluid Mech.*, **84,** 581–597.

Mellor, G. L., 1973: Analytic prediction of the properties of stratified planetary surface layers. *J. Atmos. Sci.*, **30,** 1061–1069.

——, and T. Yamada, 1974: A hierarchy of turbulence closure models for planetary boundary layers. *J. Atmos. Sci.*, **31,** 1791–1806.

——, 1977: The Gaussian cloud model relations. *J. Atmos. Sci.*, **34,** 356–358.

Sommeria, G., and J. W. Deardorff, 1977: Subgrid-scale condensation in models of nonprecipitating clouds. *J. Atmos. Sci.*, **34,** 344–355.

Wyngaard, J. C., 1973: On surface-layer turbulence. *Workshop on Micrometeorology,* D. Haugen, Ed., Amer. Meteor. Soc., 101–149.

——, W. T. Pennell, D. H. Lenschow and M. A. LeMone, 1978: The temperature-humidity covariance budget in the convective boundary layer. *J. Atmos. Sci.*, **35,** 47–58.

——, and M. A. LeMone, 1980: Behavior of the refractive index structure parameter in the entraining convective boundary layer. *J. Atmos. Sci.*, **37,** 1573–1585.

Zeman, O., and J. L. Lumley, 1976: Modeling buoyancy driven mixed layers. *J. Atmos. Sci.*, **33,** 1974–1988.